© 2020. Published by The Company of Biologists Ltd | Biology Open (2020) 9, bio047290. doi:10.1242/bio.047290

RESEARCH ARTICLE

Greb1 is required for axial elongation and segmentation in vertebrate embryos

Ravindra Singh Prajapati[1,*], Richard Mitter[1,2], Annalisa Vezzaro[1,3] and David Ish-Horowicz[1,4,‡,§]

ABSTRACT

During vertebrate embryonic development, the formation of axial structures is driven by a population of stem-like cells that reside in a region of the tailbud called the chordoneural hinge (CNH). We have compared the mouse CNH transcriptome with those of surrounding tissues and shown that the CNH and tailbud mesoderm are transcriptionally similar, and distinct from the presomitic mesoderm. Amongst CNH-enriched genes are several that are required for axial elongation, including *Wnt3a*, *Cdx2*, *Brachyury*/*T* and *Fgf8*, and androgen/oestrogen receptor nuclear signalling components such as *Greb1*. We show that the pattern and duration of tailbud *Greb1* expression is conserved in mouse, zebrafish and chicken embryos, and that *Greb1* is required for axial elongation and somitogenesis in zebrafish embryos. The axial truncation phenotype of *Greb1* morphant embryos can be explained by much reduced expression of *No tail* (*Ntl*/*Brachyury*), which is required for axial progenitor maintenance. Posterior segmentation defects in the morphants (including misexpression of genes such as *mespb*, *myoD* and *papC*) appear to result, in part, from lost expression of the segmentation clock gene, *her7*.

KEY WORDS: Tailbud, Neural tube, Axial stem cells, Somites, Transcriptome, Progenitors, Clock

INTRODUCTION

Vertebrate embryos develop in a highly organized fashion, progressively laying down axial tissues as they elongate along the anteroposterior embryonic axis (Brown and Storey, 2000; Catala et al., 1996; Wilson and Beddington, 1996; Wilson et al., 2009). Serial transplantation and other lineage tracing studies in mouse and chick have shown that a self-maintaining region in the tailbud called the chordoneural hinge (CNH) includes multipotent stem-cell-like progenitors for axial structures (Brown and Storey, 2000; Catala et al., 1996; Wilson and Beddington, 1996; Wilson et al., 2009). These include bipotent neuromesodermal progenitors (NMPs) that can generate both neural and mesodermal cells (Cambray and Wilson, 2002; Cambray and Wilson, 2007; McGrew et al., 2008; Selleck and Stern, 1991; Tam and Tan, 1992; Tzouanacou et al., 2009).

Adjacent to the CNH is the tailbud mesoderm (TBM) that contains the unsegmented precursors of the paraxial mesoderm; the presomitic mesoderm (PSM; Fig. 1A). During elongation, the PSM is displaced posteriorly while its anterior buds off a series of somites, epithelial balls that develop into segmental mesodermal structures such as the axial skeleton and musculature (reviewed in Pourquié, 2011).

Several studies have illuminated how axial progenitors are maintained during anteroposterior elongation. Briefly, a positive feedback loop between Brachyury/T and Wnt3a maintains axial progenitors in the tail bud (Martin and Kimelman, 2010; Wilson et al., 2009). In parallel, Fgf signalling protects axial progenitors from differentiation induced by retinoic acid (RA) that is secreted by differentiating and young somites and diffuses into the PSM (Diez del Corral et al., 2003; Olivera-Martinez et al., 2012; Ribes et al., 2009).

However, Fgf8, Wnt3 and T are all expressed in much larger domains than the CNH and so do not specifically distinguish axial progenitors from more specialised cells such as the TBM. Transcriptome analysis of dissected axial progenitor tissue during the period of axial elongation and of *in vitro*-derived NMPs has identified genes that are differentially expressed between progenitors and presomitic mesoderm cells (Gouti et al., 2017; Olivera-Martinez et al., 2014; Wymeersch et al., 2019). However, the functional significance of many of these genes has yet to be defined.

In this paper, we explore the transcriptional profiles of the CNH, TBM and PSM of E10.5 mouse embryos. We find that the CNH transcriptome is very similar to that of the TBM, and significantly different from that of the PSM. Several genes are expressed in both the CNH and TBM but not in the PSM, although none exclusively mark the CNH. Amongst the CNH-enriched transcripts is *Greb1*, which encodes a transcriptional co-activator for androgen/oestrogen hormone signalling. We show that *Greb1* is expressed in the tailbud in mouse, chick and zebrafish embryos, and is required for axial progenitor maintenance and somite compartmentalisation in zebrafish. Our results indicate that Greb1 plays an evolutionarily-conserved role during vertebrate axial extension and segmentation.

RESULTS AND DISCUSSION

CNH transcriptome is distinct from PSM but not TBM

To identify potential markers for the CNH, we used microarray analysis on dissected tissue regions to identify genes whose expression in the E10.5 mouse CNH is elevated relative to that in the PSM and TBM (Fig. 1A). Hierarchical clustering of the replicate transcriptome patterns confirmed that the transcriptional profiles of the CNH, PSM and TBM are distinct (Fig. 1B; see Materials and Methods). Differential gene expression analyses identified 150

[1]Cancer Research UK Developmental Genetics Laboratory, CRUK London Research Institute. [2]Francis Crick Institute, 1 Midland Rd, London NW1 1AT, UK. [3]Veyrier, 1255, Switzerland. [4]Cancer Research UK Developmental Genetics Laboratory, and University College London, UK.
*Present address: Centre for Craniofacial Development and Regenerative Biology, King's College London, London, SE1 9RT, UK. ‡Present address: Medical Research Council Laboratory of Molecular Biology, University College London, Gower St, London WC1E 6BT, UK.

§Author for correspondence (d.ish-horowicz@ucl.ac.uk)

R.S.P., 0000-0002-6173-6615; R.M., 0000-0002-1279-3760; D.I.-H., 0000-0001-5684-7129

Received 27 August 2019; Accepted 6 January 2020

Biology Open (2020) 9, bio047290. doi:10.1242/bio.047290

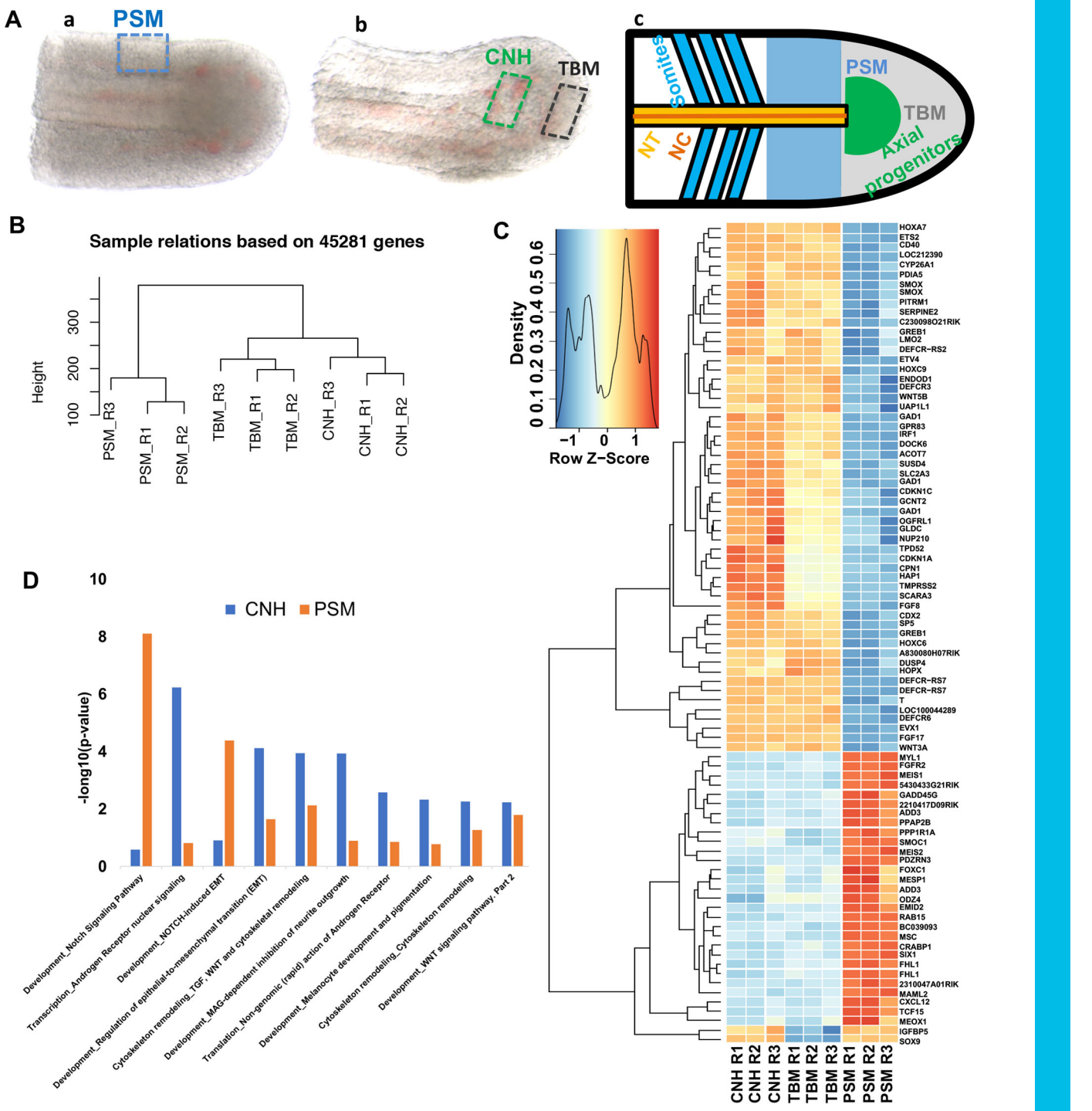

Fig. 1. CNH transcriptome is distinct from PSM. (A) Dissection of PSM, CNH and TBM of mouse at E10.5; (a) dorsal view of E10.5 tail, blue dashed rectangle represents dissected PSM and, (b) lateral view of a after removing PSM from last somite till end of tail, green dashed rectangle represents dissected CNH, black dashed rectangle represents dissected TBM; (c) schematic of tail regions with anterior to the left. Text colours correspond to those of different posterior axial regions colours (NT, neural tube; NC, notochord; PSM, presomitic mesoderm; TBM, tail bud mesoderm). Two biological and one technical replicates were performed for all three tissues (PSM, TBM and CNH). (B) A dendrogram illustrating the replicates' reproducibility, derived by hierarchical clustering of their transcriptomes (see Materials and Methods). (C) Heatmap showing differentially expressed genes (fold change >2 and <−2, and *P*-value <0.05) in the CNH, TBM and PSM. (D) Pathway enrichment analysis (see Materials and Methods). y-axis shows -$\log_{10}$(*P*-value) with enriched GO terms along the x-axis.

upregulated and 98 downregulated genes comparing the CNH to the PSM. The most significantly changed genes are listed briefly in Table 1, and the complete list can be found in Table S1. Only 12 upregulated and two downregulated transcripts distinguished the CNH and TBM, which is consistent with the latter population being directly derived from the former (Table 1; Table S1).

To confirm that many genes identified by microarray analysis are selectively expressed in progenitor regions of the extending embryo,

Biology Open (2020) 9, bio047290. doi:10.1242/bio.047290

Table 1. List of differentially expressed genes in the CNH (FDR<0.01; fold change >2 or <−2).

ILMN_Gene	CNH versus PSM fold change	CNH versus PSM FDR
DEFCR-RS7	11.9	1.96E-08
T	10.2	6.68E-05
FGF17	7.4	2.10E-09
LOC100044289	6.8	1.24E-05
WNT3A	6.0	1.62E-05
EVX1	6.0	6.83E-07
DEFCR6	5.1	1.09E-06
FGF8	4.0	1.49E-06
GREB1	3.8	5.77E-07
CDX2	3.8	3.03E-05
SP5	3.6	1.27E-06
HOXC6	3.6	4.54E-05
A830080H07RIK	3.3	3.03E-05
ETS2	3.0	3.63E-07
CPN1	2.9	3.52E-06
HOXA7	2.9	2.01E-06
CDKN1A	2.7	3.63E-07
DEFCR-RS2	2.7	5.49E-03
TPD52	2.6	2.37E-06
CD40	2.6	2.91E-05
LOC212390	2.6	7.02E-08
HOPX	2.5	1.07E-04
GAD1	2.5	3.25E-06
GCNT2	2.5	1.71E-05
C230098O21RIK	2.5	3.29E-04
GPR83	2.4	1.99E-07
LMO2	2.4	8.26E-04
DUSP4	2.4	2.03E-03
ETV4	2.3	1.15E-05
DOCK6	2.3	1.12E-06
TMPRSS2	2.3	1.21E-07
IRF1	2.3	1.29E-06
SUSD4	2.3	1.98E-05
SLC2A3	2.3	1.15E-06
SMOX	2.3	6.56E-05
CDKN1C	2.3	1.03E-04
UAP1L1	2.3	1.67E-03
SERPINE2	2.3	4.93E-03
CYP26A1	2.2	2.32E-04
GLDC	2.2	1.20E-04
PITRM1	2.2	4.98E-04
ACOT7	2.2	3.00E-05
HAP1	2.2	5.77E-07
WNT5B	2.2	1.01E-05
SCARA3	2.2	1.43E-06
PDIA5	2.2	2.64E-05
ENDOD1	2.2	5.38E-04
NUP210	2.1	1.45E-03
DEFCR3	2.1	1.23E-04
OGFRL1	2.1	3.55E-04
HOXC9	2.0	7.68E-06
HOXA11S	2.0	1.49E-06
CRIP2	2.0	9.04E-05
2610027C15RIK	2.0	4.67E-06
Genes downregulated in the CNH		
GPX2	−2.0	1.71E-05
EFNA5	−2.0	1.52E-06
SLC9A3R1	−2.0	1.42E-04
GADD45G	−2.0	1.05E-03
2310047A01RIK	−2.1	1.52E-06
MESP1	−2.1	5.00E-03
FHL1	−2.1	2.43E-06
CRABP1	−2.1	1.56E-06
BC039093	−2.2	9.63E-06
MSC	−2.2	1.03E-06
FOXC1	−2.2	5.53E-03
SIX1	−2.2	1.52E-06
ADD3	−2.2	8.09E-04
SMOC1	−2.3	1.72E-06
EMID2	−2.5	1.90E-05
RAB15	−2.5	3.22E-08
MAML2	−2.6	2.37E-06
PPP1R1A	−2.7	2.57E-05
5430433G21RIK	−2.8	1.12E-06
PPAP2B	−2.8	3.48E-05
MEIS1	−3.0	3.25E-06
MYL1	−3.4	5.77E-07
2210417D09RIK	−3.4	3.25E-06
FGFR2	−3.7	5.07E-08
MEIS2	−4.0	3.25E-06
MEOX1	−4.7	5.31E-03
PDZRN3	−4.8	3.63E-07
CXCL12	−5.5	9.87E-05
TCF15	−5.8	2.09E-05
ILMN_Gene	**CNH versus TBM.FC**	**CNH versus TBM.FDR**
IGFBP5	2.4	4.23E-03
SOX9	2.1	3.03E-05

Genes marked with * are differentially expressed in the CNH comparison to TBM and PSM (fold change >1.5 or <−1.5). Genes with FDR <0.01 and fold change >1.5 and <−1.5. The detailed data for all expression differences with FC >1.5, or <−1.5 are presented in Table S1.

we searched the Mouse Genome Informatics (MGI) database (Finger et al., 2017) for the expression patterns of 53 genes whose expression were upregulated ≥2-fold in the CNH (Fig. 1C). A majority of these genes (29/53) are annotated as being expressed in tissues related to axial elongation, i.e. in one or more of the primitive streak, node, tailbud and future spinal cord (Table 2; Table S2). By contrast, most downregulated genes (23/27 reduced ≥2-fold) are expressed in more specialised progeny cells, i.e. somites, unsegmented mesoderm or neural tube (Table 2; Table S2).

Greb1 expression coincides with axial elongation in vertebrate embryos

We also compared our list of CNH-enriched genes with those previously identified in previous studies of the CNH or NMPs (Table S3; Gouti et al., 2017; Olivera-Martinez et al., 2014; Wymeersch et al., 2019). Expression of seven of the ten most-enriched genes (*Fgf8*, *Cdx2*, *T*, *Wnt3a*, *Sp5*, *Evx1* and *Fgf17*) was previously reported in the CNH and TBM, and to be functionally important for axial development (Cambray and Wilson, 2007; Dunty et al., 2014; Maruoka et al., 1998; Takada et al., 1994).

The expression and roles of the two most CNH-enriched genes from our study [*Defcr-rs7*, *Defcr-rs6* (which encode small immune-defect peptides)] during axial elongation and segmentation remains to be studied. *Greb1*, which encodes a co-activator of the oestrogen and androgen receptors that is active in human oestrogen-receptor-positive primary breast and prostate cancer cells (Lee et al., 2019; Mohammed et al., 2013), is another top CNH enriched gene. Indeed, androgen receptor nuclear signalling is the most CNH-enriched pathway revealed by pathway enrichment analysis of our differentially expressed genes (Fig. 1D; Table S4; see Materials and Methods). Other androgen-responsive genes also enriched in the CNH include *P21*, *cyclinD1* and *MMP2* (Table S3). Indeed, the MMP2 matrix metalloproteinase is required for axial elongation – morpholino knockdown of *MMP2* in zebrafish embryos – results in

Biology Open (2020) 9, bio047290. doi:10.1242/bio.047290

Table 2. Annotated gene expression patterns (E7.5–13.5 mouse embryos) for genes that are differentially expressed in the CNH

Gene	Anatomical regions
Gene upregulated in CNH >2-fold change and FDR <−0.01	
Acot7	Future spinal cord
Cdkn1a	Neural tube, somite, dermomyotome, myotome, dermomyotome, somite, future spinal cord, somite
Cdkn1c	Somite, dermomyotome, future spinal cord
Cdx2	Tail bud, future spinal cord neural plate, neural tube, tail unsegmented mesenchyme, neural tube, tail mesenchyme
Cpn1	Neural tube
Cyp26a1	Future spinal cord neural plate, migrating neural crest, tail bud, tail mesenchyme, tail neural plate, tail neural tube, tail sclerotome
Dock6	Future spinal cord, tail unsegmented mesenchyme
Dock7	Somite
Dusp4	Future spinal cord, tail unsegmented mesenchyme
Ets2	Primitive streak, neural tube, somite, trunk somite, future spinal cord, tail unsegmented mesenchyme
Etv4	Future spinal cord, primitive streak, future spinal cord neural plate, tail bud, dermomyotome, sclerotome, neural tube floor plate, future spinal cord
Evx1	Primitive streak, primitive streak, primitive streak, primitive streak, tail bud, tail mesenchyme, future spinal cord, future spinal cord, neural tube, future spinal cord
Fgf8	Future spinal cord, primitive streak, future spinal cord neural plate, somite, tail bud, trunk somite, tail mesenchyme, tail unsegmented mesenchyme, tail neural plate, trunk dermomyotome, myotome, tail somite, neural tube
fgf17	Tail somite, somite, primitive streak, tail mesenchyme, tail unsegmented mesenchyme, neural tube
Gad1	Neural tube, tail bud, tail mesenchyme, tail paraxial mesenchyme, tail future spinal cord, tail neural tube, future spinal cord
Gcnt2	Future spinal cord
Gldc	Neural lumen
Greb1	Future spinal cord
Hopx	Tail unsegmented mesenchyme and neural tube basal columns
Hoxa7	Neural tube ventricular layer, trunk somite, somite, neural tube, tail paraxial mesenchyme
Hoxc6	Neural tube, somite, primitive streak, trunk somite
Hoxc9	Tail paraxial mesenchyme, neural tube, trunk somite, tail somite
Lmo2	Neural tube and head somites
Pitrm1	Somite and neural tube
Serpine2	Trunk dermomyotome and neural tube
Slc2a3	Neural tube
Sp5	Future spinal cord, somite, primitive streak, head somite, trunk somite, future spinal cord neural plate, neural tube, tail unsegmented mesenchyme, dermomyotome, tail somite, neural tube lateral wall, tail mesenchyme
T	Dermomyotome, primitive streak, node, future spinal cord neural plate, tail neural tube, tail bud, tail mesenchyme, tail unsegmented mesenchyme, tail neural plate, caudal neuropore, neural tube
Wnt3a	Tail bud, primitive streak, future spinal cord, tail mesenchyme, tail unsegmented mesenchyme, neural tube, neural tube roof plate, neural tube lateral wall, sclerotome, neural tube floor plate
Wnt5b	Neural tube floor plate, future spinal cord, neural tube
Genes downregulated in CNH<−2-fold change FDR<−0.01	
Add3	Tail unsegmented mesenchyme
Cfh	Future spinal cord
Crabp1	Neural crest, neural tube, head somite, trunk somite, migrating neural crest, trunk sclerotome, neural tube lateral wall, future spinal cord, primitive streak, trunk unsegmented mesenchyme, anterior pro-rhombomere neural crest, future hindbrain posterior to rhombomere 5 neural crest, posterior pro-rhombomere neural crest, rhombomere 1 neural crest, rhombomere 2 neural crest, rhombomere 5 neural crest, future spinal cord neural fold, neural tube floor plate, future midbrain neural crest, future diencephalon neural crest, prosencephalon neural crest, tail bud, trunk dermomyotome, somite, neural tube roof plate
Cxcl12	Future spinal cord
Fgfr2	Primitive streak, head somite, trunk somite, neural tube, neural tube lateral wall, myotome, sclerotome
Foxc1	Primitive streak, node, future spinal cord, trunk paraxial mesenchyme, head somite, trunk somite, trunk unsegmented mesenchyme, neural tube, somite, tail unsegmented mesenchyme, trunk dermomyotome, trunk sclerotome, tail sclerotome
Gadd45g	Trunk unsegmented mesenchyme, neural fold, trunk unsegmented mesenchyme, future spinal cord neural fold, tail unsegmented mesenchyme, neural tube, tail unsegmented mesenchyme, myotome, neural tube
Ism1	Somite, trunk unsegmented mesenchyme, somite, somite, tail unsegmented mesenchyme, neural tube, dermomyotome
Maml2	Neural tube
Meis1	Trunk somite, future spinal cord, trunk paraxial mesenchyme, somite, neural plate, neural fold, neural groove, trunk unsegmented mesenchyme, neural tube, trunk myotome, trunk sclerotome, myotome, sclerotome, neural tube floor plate, neural tube mantle layer
Meis2	Neural plate, neural fold, neural groove, trunk unsegmented mesenchyme, neural tube, somite, future spinal cord, trunk somite, trunk myotome, trunk sclerotome, myotome, sclerotome, neural tube floor plate, neural tube mantle layer
Meox1	Primitive streak, trunk paraxial mesenchyme, head somite, trunk somite, trunk unsegmented mesenchyme, somite, dermomyotome, sclerotome, trunk dermomyotome, trunk sclerotome, trunk myotome, neural tube, tail somite, tail unsegmented mesenchyme, unsegmented mesenchyme
Mesp1	Primitive streak, trunk unsegmented mesenchyme, tail unsegmented mesenchyme, trunk somite
Msc	Trunk and tail dermomyotome
Myl1	Somite, myotome, trunk somite, tail paraxial mesenchyme
Pdzrn3	Tail somite, tail unsegmented mesenchyme
Plpp3	Neural tube ventricular layer, somite, myotome
Ppp1r1a	Neural tube, node, somite
Rab15	Neural tube
Six1	Trunk somite, trunk unsegmented mesenchyme, tail unsegmented mesenchyme, somite
Smoc1	Node, somite, primitive streak
Tcf15	Primitive streak, head somite, trunk paraxial mesenchyme, trunk unsegmented mesenchyme, trunk somite, somite, tail paraxial mesenchyme, tail unsegmented mesenchyme, dermatome, myotome, sclerotome, tail sclerotome, trunk dermomyotome, dermomyotome, trunk sclerotome
Tenm4	Future brain neural fold, future spinal cord neural plate, future spinal cord neural fold, trunk somite, somite, tail somite

Expression patterns were extracted from the Mouse Genome Informatics (MGI) database. Details of the data, including references, are reported in Table S2.

Biology Open (2020) 9, bio047290. doi:10.1242/bio.047290

severe axial truncations (Zhang et al., 2003). Further studies will be required to test if androgen signalling operates in axial patterning.

Expression of chick *Greb1* in the axial stem cell zone has been described previously (Olivera-Martinez et al., 2014). We expanded this finding by examining *Greb1* expression during segmentation, using three different vertebrate systems. First, we visualised *Greb1* transcription in elongating mouse embryos using *in situ* hybridisation (E10.5–E13.5; see Materials and Methods). In early (E8.5) embryos, *Greb1* is expressed in a posterior domain that encompasses the caudal lateral epiblast, the region that includes the axial progenitors (Fig. 2A,A′). By E10.5, labelling is restricted to the CNH and dorsal TBM (Fig. 2B,B′). Expression in these regions is maintained during axial elongation, albeit more weakly by E12.5, and is lost at E13.5 when axial elongation ceases (Fig. 2C,D).

The above results show that, although not restricted to the CNH, axial *Greb1* transcription in early mouse embryos coincides in time and place with the processes of axial extension and segmentation. To test if this correlation is evolutionarily conserved, we examined *Greb1* expression in chick and zebrafish embryos. In both animals, *Greb1* expression in the tailbud starts during elongation, and terminates when elongation and segmentation is complete. *Greb1* is expressed in the HH13 chick caudal neural plate, whose cells contribute to the neural tube, somites and notochord, node and primitive streak (Fig. 2E,E′). Its axial transcription then becomes confined to the region of the tailbud which includes the chick CNH and TBM (HH17; Fig. 2F; McGrew et al., 2008), and has almost completely decayed when elongation is complete (HH26; Fig. 2G).

In zebrafish embryos, *Greb1* transcription becomes confined to the region of the tailbud that contains axial progenitors (Fig. 2H–L). It persists during segmentation (11–16 hpf; Fig. 2I–K), and disappears when axial elongation comes to an end (24 hpf; Fig. 2L). This conserved spatial and temporal time course in early vertebrate embryos strengthens the link between *Greb1* expression and axial extension.

Knockdown of *GREB1* disrupts axial elongation

To test if *Greb1* is functionally required during elongation and segmentation, we knocked down its expression by injecting antisense morpholinos into 1–2-cell zebrafish embryos (see Materials and Methods). We used two *Greb1* splicing-blocking morpholinos (M1 and M2) that target the exon2-intron2 and exon16-intron16 boundaries, respectively (Fig. S1). These oligos should interfere with mRNA splicing to cause skipping of the adjacent exon and a shifted translational reading frame. The ensuing premature translational termination would completely truncate Greb1 protein (M1) or encode one that is only 40% full-length

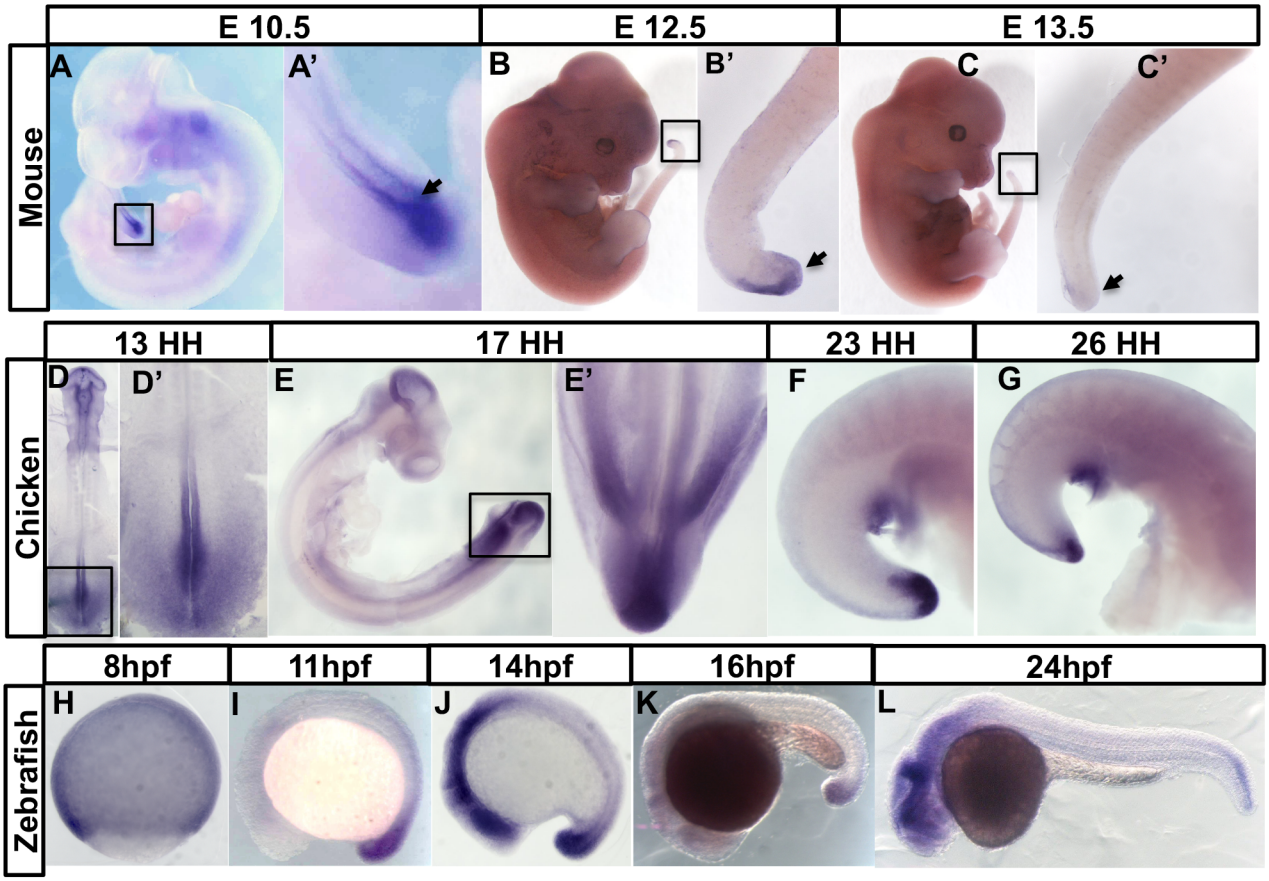

Fig. 2. The timing of axial *Greb1* expression is coincident with axial elongation in vertebrate embryos. (A–D) Mouse embryos and their tail regions at different embryonic stages. (A,A′) Dorsal view of E8.5 embryo showing expression in the caudal lateral epiblast (CLE). PS: primitive streak. (B,B′) Lateral view of E10.5 embryo, showing the *Greb1*-expressing tail region. (C) Lateral view of E12.5 tail region, showing reduced *Greb1* expression. (D) Lateral view of E13.5 tail region, showing that expression is lost. (E–F) *Greb1* expression in chick embryos at different stages: (E,E′) dorsal views of HH13 embryo and its tail region; (F) lateral and (F′) ventral view of a tail region at HH17; (G) lateral view of HH26 embryo, showing that *Greb1* expression in the tailbud is almost gone. H–L are lateral views of zebrafish embryos of the indicated ages (hpf, hours post-fertilisation). Each pattern was analysed in two independent experiments using, for each stage, at least five mouse, or 10–15 chicken or zebrafish embryos. Tailbud regions are arrowed. Boxes in lower magnification images show the tail regions with magnified views in the adjacent panel.

Biology Open (2020) 9, bio047290. doi:10.1242/bio.047290

(M2). As a control, we also injected a mismatched morpholino (MM) based on M2 but with five bases mutated to prevent binding to the primary *Greb1* transcript.

We verified the splice-blocking activities of both morpholinos via RT-PCR on RNA from injected embryos. *Greb1* splice variants corresponding to misprocessed transcripts were detected in M1- and M2-injected morphants but not MM morphant embryos (Fig. S1). DNA sequencing of these variant products confirmed that they result from skipping of the appropriate exons: exon 2 for oligo M1, and exon16 for M2 (Fig. S1).

We assayed the effects of *Greb1* knockdown 24 h after injection into embryos, when extension and segmentation is complete. M1 and M2 morphant embryos suffer three major axial defects: a curved trunk; a reduction in total body length (head-to-tail); misshaped somites and indistinct somite boundaries predominantly in more posterior axial regions (Fig. 3A–C). Injection of 4 ng/µl blocking oligonucleotide generates a high frequency of embryos showing all three defects (50/107 injected embryos for M1; 61/110 embryos for M2). No such abnormalities are seen in embryos injected with the control MM morpholino (0/15). Injecting 2 ng/µl of morpholino causes similar defects, albeit at lower frequencies (M1: 11/46; M2: 15/36; MM: 0/8).

These phenotypes are not due to unspecific toxicity from the injection. We co-injected each morpholino with one that knocks down *p53* expression, thereby preventing previously reported oligo-induced p53-dependent cell death (see Materials and Methods; Robu et al., 2007). Each blocking morpholino still efficiently caused axial extension and segmentation phenotypes (M1: 20/30; M2: 25/37; control MM: 0/10). Together, our data suggest that normal axial elongation and segmentation are dependent on Greb1 activity.

Greb1 is needed to maintain *Ntl* expression in the tailbud

The axial truncations of *Greb1* morphants resembles the phenotype of embryos mutant for *No tail* (*Ntl*), the zebrafish homologue of *Brachyury/T*, which is expressed in the tailbud, posterior PSM and notochord of wild-type embryos (Halpern et al., 1993; Schulte-Merker et al., 1994). *Ntl* in the tailbud helps maintain axial progenitors by protecting them from premature differentiation induced by RA secreted by the anterior PSM and somites (Diez del Corral et al., 2003; Martin and Kimelman, 2010; Olivera-Martinez et al., 2012; Ribes et al., 2009).

Tailbud *Ntl* expression in *Greb1* morphants is indeed much lower than in wild-type or control embryos (M2: 20/34; MM: 0/11; Fig. 3Q′,R,R′). Thus, *Greb1* is required for efficient *Ntl* expression, and reduced *Ntl* levels can explain the morphant embryos' truncated axis.

Greb1 depletion affects somite polarity via the segmentation clock

During axial segmentation in zebrafish embryos, a linear array of chevron-shaped somites is progressively generated from the PSM between 10–24 hpf (Fig. 3A,A′). As mentioned above, *Greb1* morphants lack morphologically discrete somites (Fig. 3A–C).

To assess if this morphological phenotype is accompanied by altered gene expression at somite boundaries, we examined *xirp2a/cb1045*, which is expressed in the myoseptum between myotomes (Deniziak et al., 2007; Schroter and Oates, 2010). Strong distinct posterior stripes of *Xirp2a* mRNA expression are frequently lost in *Greb1* morphant embryos (M1: 20/25; M2: 14/18; MM: 0/15; Fig. 3A–C), corresponding to the regions with abnormal somite appearance.

In wild-type embryos, boundaries arise between posterior and anterior compartments of adjacent somites, raising the possibility that *Greb1* is needed for somite compartmentalisation. To test this idea, we studied *myoD* transcripts, which are normally expressed in the posterior half of each somite (Weinberg et al., 1996). By contrast, expression of *myoD* extends into the anterior compartment in *Greb1* morphants (M1: 7/15; M2: 13/18; MM: 0/18; Fig. 3D–F), suggesting that anterior morphant cells have adopted a posterior character. M1 and M2 morphants show similar effects on axial morphology and *Xirp2a* and *myoD* expression, we only analysed M2 morphants in subsequent experiments.

Analysing *papC*, which is expressed in the anterior compartments of newly formed somites (Rhee et al., 2003) provides additional support for the idea that *Greb1* contributes to the establishment of anterior compartmentalisation. In morphant embryos, *papC* levels are reduced and lack clear borders (M2:14/22; MM:0/22; Fig. 3G,L).

Expression of *myoD* is normally suppressed in anterior somite compartments by *mespb*, which together with *mespa*, is expressed there in newly-formed somites (Sawada et al., 2000). We examined expression of both *mesp* genes in the morphant embryos and found that, although *mespa* expression is not altered (M2: 0/24; MM:0/21; Fig. 3H,M), *mespb* expression is greatly lowered (M2: 6/10; MM: 0/21; Fig. 3I,N). This reduction explains why *myoD* is derepressed in *Greb1* morphants, and reinforces our view that *Greb1* is needed for somite compartmentalisation.

What might cause mis-specification of somite compartments? During vertebrate axial extension, the regular production of equal-sized segments results from the action of a molecular oscillator ('segmentation clock'), which drives cyclic transcription of many PSM genes with a period corresponding to that of somite formation (Dequeant et al., 2006; Niwa et al., 2007; Palmeirim et al., 1997; Pourquié, 2011). Together, axial extension and cyclic gene expression establish reiterated expression of genes that define somite compartmentalisation and, hence, somite boundaries.

We examined two such cycling genes, *her1* and *her7*, which encode transcriptional repressors whose periodic expression in the zebrafish PSM form and pattern the somites (Oates and Ho, 2002; Pourquié, 2011; Takke and Campos-Ortega, 1999). In particular, *her7* is a regulator of *mespb* expression in forming somites (Choorapoikayil et al., 2012; Oates and Ho, 2002). Expression of *her1* is normal in the PSMs of *Greb1* morphant embryos (M2 0/16; MM 0/19; Fig. 3J,O), but that of *her7* is lost, in both the tailbud and PSM (M2 5/5; MM 0/5; Fig. 3K,P). The latter's loss explains the reduced *mespb* expression and abnormal somite compartmentalisation in *Greb1* morphant embryos.

Together, our experiments support the following model for the *Greb1* morphant phenotypes (Fig. 3S). Axial extension is truncated due to reduced expression of *Ntl* and, thereby, loss of axial progenitors (Fig. 3Q,Q′,R; Martin and Kimelman, 2010), and the segmentation phenotype is caused by loss of *her7*. This model is consistent with the misregulation of *mespb* and loss of more posterior somite boundaries in both *her7* mutants and *Greb1* morphants (Fig. 3A–F, A′–F′; Oates and Ho, 2002). Although we cannot completely exclude the possibility that the morphant morphological and molecular phenotypes are due to off-target knockdowns, this explanation seems unlikely. Each of the splice-blocking morpholinos was independently derived, and so they would not be expected affect similar sets of off-target transcripts. The combination of morphant phenotypes we observe has not previously been described, and we have also shown that they are not due to non-specific morphant toxicity. Future experiments using

Biology Open (2020) 9, bio047290. doi:10.1242/bio.047290

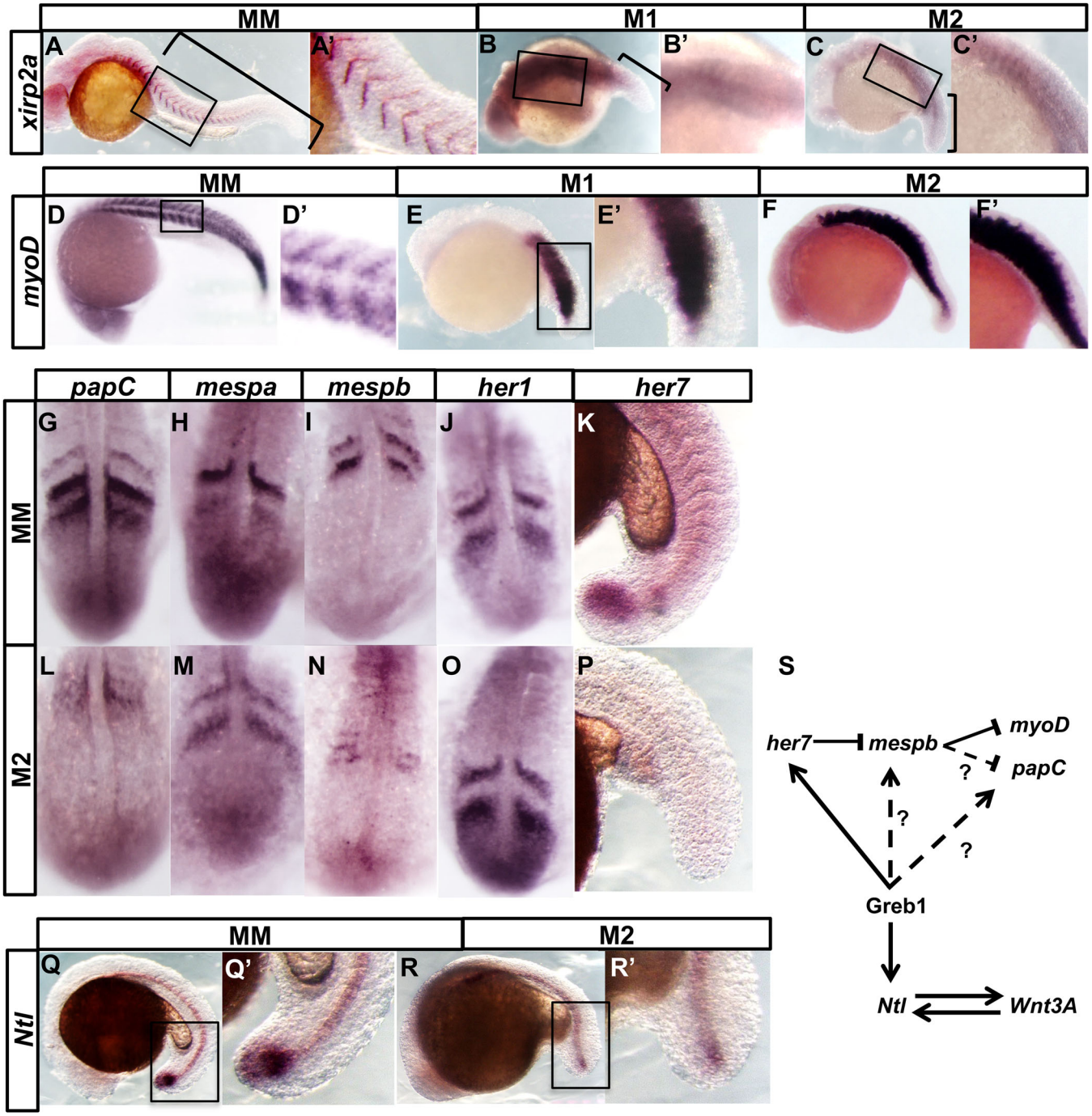

Fig. 3. *Greb1* is required for axial elongation. (A–C,A′–C′) Lateral views of zebrafish embryos at 24 hpf, showing: (A) wild-type chevrons of *xirp2a* expression and the tail region (bracketed); (B,C) posterior loss in M1 and M2 morphants. The tail regions that are truncated and contain disrupted somites are bracketed. (D–F,D′–F′): expression of *myoD* in control (MM, M1 and M2 morphants). (G,L) *papc*, (H,M) *mespa*, (I,N) *mespb*, (J,O) *her1*, (K,P) *her7* (Q,R) and (Q′,R′) *Ntl* expression in the tail region of 15 hpf control and morphant embryos. (S) A tentative model for gene interactions between Greb1 and patterning genes. Anterior expression of Her7 restricts *mespb* expression to the posterior somite compartment, which, in turn, restricts *myoD* and *papC* expression to the anterior compartment. Continuous arrows indicate interactions shown by others as likely to be direct. Dashed arrows could be direct or indirect.

CRISPR/Cas9 gene-editing will clarify this point and allow further studies of *Greb1* action.

As Greb1, Ntl and Her7 are all transcription factors, some of the effects on gene transcription that we observe may be direct. Greb1 is required for clock output via *her7*, and may also act directly on *mespb*. However, the oscillator circuitry remains intact: morphants retain cyclic *her1* expression and low level, metameric *xirp2* expression (Fig. 3B,C,J,O). The latter idea would explain why *mespb* expression is abolished in the *Greb1* morphants (Fig. 3I,N). Although further experiments will be required to distinguish between direct and indirect actions of *Greb1* and its potential targets, the evolutionarily conserved pattern and time-course of *Greb1* expression that we have shown in mouse, chick and zebrafish (Fig. 2) suggest that *Greb1* is an important component in vertebrate axial patterning.

Biology Open (2020) 9, bio047290. doi:10.1242/bio.047290

MATERIALS AND METHODS

Maintenance and collection of embryos

E10.5 mouse embryos were collected from *CD1* and *C57Bl/6J* pregnant females (Charles River Laboratories International Inc., UK) in M2 media (Sigma-Aldrich, M7167). Fertilized chicken eggs from Henry Stewart & Co (Louth, UK) were incubated at 37°C, and embryos were staged according to Hamburger and Hamilton (Hamburger and Hamilton, 1992). Adult wild-type zebrafish were maintained at 27°C on a regular 14 h light/10 h dark cycle, and embryos were collected and staged as described by Kimmel et al. (Kimmel et al., 1995). *p53* heterozygous and homozygous mutant zebrafish embryos were obtained by crossing *p53* homozygous female to *p53* heterozygous males (Robu et al., 2007). Animals used in this study were handled by professionals meeting all the requirements of the Animals (Scientific Procedures) Act 1986.

Transcription profiling

Mouse CNH, PSM and TBM explants per experiment were dissected as previously described (Fig. 1A; Cambray and Wilson, 2002). Approximately 50 pieces of each region were pooled, and total RNA extracted using the RNeasy Mini Kit (Qiagen, cat. no. 74104). Before processing the RNA samples for microarray analysis, their quality was tested using the Bioanalyzer RNA 6000 Pico kit (Agilent, cat. no. 5067-1513). Samples with RNA integrity number (RIN) 8–10 were processed for transcriptional profiling at the Genome Centre (Blizard Institute, Barts and the London School of Medicine and Dentistry) using Illumina 'Ref6v2' beads arrays. Two biological and one technical replicate were carried out for each region – CNH, TBM and PSM.

Microarray data analysis

Analysis was performed using software packages developed for Bioconductor version 2.4.0 and R version 2.9.0. The Illumina dataset were processed using the probe intensity transformation (VST) and normalization (RSN) methods from the 'lumi' package (Ihaka and Gentleman, 1996; Team, 2009). Hierarchical clustering was used to assay the reproducibility of the biological replicates. Differential gene expression was assessed between tissue-type replicate groups using an empirical Bayes' *t*-test as implemented in the 'limma' package and taking account of replicate group and batch effects (K., 2005). Three comparisons were performed: CNH versus PSM, CNH versus TBM, CNH versus Combined PSM and TBM. The resulting *P*-values were adjusted to control the false discovery rate (FDR) using the Benjamini and Hochberg method. Two lists of differentially expressed genes were produced using different thresholds: (1) all genes that exhibited FDR<0.05 in all three comparisons, or a fold change >1.5 in the same direction in all three contrasts were classified as differentially expressed. (2) 'Top50': genes were selected on the basis of FDR<0.05 and an absolute fold change ≥1.5 from the CNH versus PSM comparison, ordered by fold change, and the top 50 most-changed genes were selected and clustered using hierarchical clustering algorithm. Genes from the two lists were combined and used to perform a pathway enrichment and network analysis with MetaCore software from Clarivate Analytics.

In situ hybridisation

We visualised spatiotemporal transcript expression in mouse, chick and zebrafish embryos by *in situ* hybridisation using digoxigenin-labelled antisense RNA probes (Hanisch et al., 2013; Rallis et al., 2010; Stauber et al., 2009). In general, templates for making antisense RNA probes for *in situ* detection of *Greb1* transcripts were generated by RT-PCR of embryonic mRNA, cloning into *PCR2.1-TOPO-TA* vector (Invitrogen; Table S5), linearization using *Spe1* or *Not1*, and transcription by T3 or T7 RNA polymerase. cDNA templates for generating other antisense-RNA probes were obtained from the Julian Lewis lab. Expression patterns were replicated and scored independently by at least two people.

Morpholino injection

To knockdown zebrafish *Greb1* expression, we injected 2 nl of the following splicing-blocking morpholinos into 1–2-cell embryos at 2–8 ng/µl in 0.4 mM $MgSO_4$, 0.6 mM $CaCl_2$, 0.7 mM KCl, 58 mM NaCl, 5 mM HEPES pH 7.6; 0.05% Phenol Red: (M1) 5′-GGAAGACTGTAAAAGC-TCACCCTCA-3′, (M2) 5′AATACTGAAATCACACCTCTCCTCC-3′ (Fig. S1; Gene Tools, Philomath, OR, USA). Control injections used a mutated M2 oligo (MM) with five nucleotide mismatches: 5′-AATAGTC-AAATCAGACCTGTGCTCC-3′. To test for non-specific toxicity, 4 ng/µl of blocking or control morpholino was co-injected with 6 ng/µl *p53* antisense morpholino (Robu et al., 2007). Efficacy and specificity were tested by sizing and sequencing RT-PCR products of total RNA from morpholino-injected embryos, SuperScript III One-Step RT-PCR mix (Invitrogen, #12574035).

Acknowledgements

We thank the CR-UK Developmental Genetics Laboratory members and Andrea Streit for comments on the paper. Val Wilson provided advice and training, generous help with CNH dissections and key criticisms of a previous draft of the paper.

Competing interests

The authors declare no competing or financial interests.

Author contributions

Conceptualization: R.S.P., D.I.-H.; Methodology: R.S.P.; Validation: R.S.P.; Formal analysis: R.M.; Investigation: R.S.P., A.V.; Data curation: R.M.; Writing - original draft: D.I.-H.; Writing - review & editing: R.S.P., R.M., D.I.-H.; Visualization: R.S.P.; Supervision: D.I.-H.; Project administration: R.S.P.; Funding acquisition: D.I.-H.

Funding

The work was funded by Cancer Research UK and University College London.

Data availability

The non-normalised and normalized expression sequencing data and gene tables are available from the Gene Expression Omnibus (GEO) with accession number GSE141519.

Supplementary information

Supplementary information available online at
http://bio.biologists.org/lookup/doi/10.1242/bio.047290.supplemental

References

Brown, J. M. and Storey, K. G. (2000). A region of the vertebrate neural plate in which neighbouring cells can adopt neural or epidermal fates. *Curr. Biol.* **10**, 869-872. doi:10.1016/S0960-9822(00)00601-1

Cambray, N. and Wilson, V. (2002). Axial progenitors with extensive potency are localised to the mouse chordoneural hinge. *Development* **129**, 4855-4866.

Cambray, N. and Wilson, V. (2007). Two distinct sources for a population of maturing axial progenitors. *Development* **134**, 2829-2840. doi:10.1242/dev.02877

Catala, M., Teillet, M. A., De Robertis, E. M. and Le Douarin, M. L. (1996). A spinal cord fate map in the avian embryo: while regressing, Hensen's node lays down the notochord and floor plate thus joining the spinal cord lateral walls. *Development* **122**, 2599-2610.

Choorapoikayil, S., Willems, B., Ströhle, P. and Gajewski, M. (2012). Analysis of her1 and her7 mutants reveals a spatio temporal separation of the somite clock module. *PLoS ONE* **7**, e39073. doi:10.1371/journal.pone.0039073

Deniziak, M., Thisse, C., Rederstorff, M., Hindelang, C., Thisse, B. and Lescure, A. (2007). Loss of selenoprotein N function causes disruption of muscle architecture in the zebrafish embryo. *Exp. Cell Res.* **313**, 156-167. doi:10.1016/j.yexcr.2006.10.005

Dequeant, M.-L., Glynn, E., Gaudenz, K., Wahl, M., Chen, J., Mushegian, A. and Pourquié, O. (2006). A complex oscillating network of signaling genes underlies the mouse segmentation clock. *Science* **314**, 1595-1598. doi:10.1126/science.1133141

Diez del Corral, R., Olivera-Martinez, I., Goriely, A., Gale, E., Maden, M. and Storey, K. (2003). Opposing FGF and retinoid pathways control ventral neural pattern, neuronal differentiation, and segmentation during body axis extension. *Neuron* **40**, 65-79. doi:10.1016/S0896-6273(03)00565-8

Dunty, W. C., Jr, Kennedy, M. W., Chalamalasetty, R. B., Campbell, K. and Yamaguchi, T. P. (2014). Transcriptional profiling of Wnt3a mutants identifies Sp transcription factors as essential effectors of the Wnt/beta-catenin pathway in neuromesodermal stem cells. *PLoS ONE* **9**, e87018. doi:10.1371/journal.pone.0087018

Finger, J. H., Smith, C. M., Hayamizu, T. F., McCright, I. J., Xu, J., Law, M., Shaw, D. R., Baldarelli, R. M., Beal, J. S., Blodgett, O. et al. (2017). The mouse Gene Expression Database (GXD): 2017 update. *Nucleic Acids Res.* **45**, D730-D736. doi:10.1093/nar/gkw1073

Gouti, M., Delile, J., Stamataki, D., Wymeersch, F. J., Huang, Y., Kleinjung, J., Wilson, V. and Briscoe, J. (2017). A gene regulatory network balances neural and mesoderm specification during vertebrate trunk development. *Dev. Cell* **41**, 243-261.e247. doi:10.1016/j.devcel.2017.04.002

Halpern, M. E., Ho, R. K., Walker, C. and Kimmel, C. B. (1993). Induction of muscle pioneers and floor plate is distinguished by the zebrafish no tail mutation. *Cell* **75**, 99-111. doi:10.1016/S0092-8674(05)80087-X

Hamburger, V. and Hamilton, H. L. (1992). A series of normal stages in the development of the chick embryo. 1951. *Dev. Dyn.* **195**, 231-272. doi:10.1002/aja.1001950404

Hanisch, A., Holder, M. V., Choorapoikayil, S., Gajewski, M., Ozbudak, E. M. and Lewis, J. (2013). The elongation rate of RNA polymerase II in zebrafish and its significance in the somite segmentation clock. *Development* **140**, 444-453. doi:10.1242/dev.077230

Ihaka, R. and Gentleman, R. R. (1996). A language for data analysis and graphics. *J. Comput. Graph. Stat.* **5**, 299-314. doi:10.1080/10618600.1996.10474713

K., S. G. (2005). "Limma: linear models for microarray data". In *Bioinformatics and Computational Biology Solutions Using R and Bioconductor* (ed. R. Gentleman, V. Carey, S. Dudoit, R. Irizarry and W. Huber), pp. 397-420. New York: Springer.

Kimmel, C. B., Ballard, W. W., Kimmel, S. R., Ullmann, B. and Schilling, T. F. (1995). Stages of embryonic development of the zebrafish. *Dev. Dyn.* **203**, 253-310. doi:10.1002/aja.1002030302

Lee, E., Wongvipat, J., Choi, D., Wang, P., Lee, Y. S., Zheng, D., Watson, P. A., Gopalan, A. and Sawyers, C. L. (2019). GREB1 amplifies androgen receptor output in human prostate cancer and contributes to antiandrogen resistance. *Elife* **8**, e41913. doi:10.7554/eLife.41913

Martin, B. L. and Kimelman, D. (2010). Brachyury establishes the embryonic mesodermal progenitor niche. *Genes Dev.* **24**, 2778-2783. doi:10.1101/gad.1962910

Maruoka, Y., Ohbayashi, N., Hoshikawa, M., Itoh, N., Hogan, B. L. and Furuta, Y. (1998). Comparison of the expression of three highly related genes, Fgf8, Fgf17 and Fgf18, in the mouse embryo. *Mech. Dev.* **74**, 175-177. doi:10.1016/S0925-4773(98)00061-6

McGrew, M. J., Sherman, A., Lillico, S. G., Ellard, F. M., Radcliffe, P. A., Gilhooley, H. J., Mitrophanous, K. A., Cambray, N., Wilson, V. and Sang, H. (2008). Localised axial progenitor cell populations in the avian tail bud are not committed to a posterior Hox identity. *Development* **135**, 2289-2299. doi:10.1242/dev.022020

Mohammed, H., D'Santos, C., Serandour, A. A., Ali, H. R., Brown, G. D., Atkins, A., Rueda, O. M., Holmes, K. A., Theodorou, V., Robinson, J. L. et al. (2013). Endogenous purification reveals GREB1 as a key estrogen receptor regulatory factor. *Cell Rep.* **3**, 342-349. doi:10.1016/j.celrep.2013.01.010

Niwa, Y., Masamizu, Y., Liu, T., Nakayama, R., Deng, C.-X. and Kageyama, R. (2007). The initiation and propagation of Hes7 oscillation are cooperatively regulated by Fgf and notch signaling in the somite segmentation clock. *Dev. Cell* **13**, 298-304. doi:10.1016/j.devcel.2007.07.013

Oates, A. C. and Ho, R. K. (2002). Hairy/E(spl)-related (Her) genes are central components of the segmentation oscillator and display redundancy with the Delta/Notch signaling pathway in the formation of anterior segmental boundaries in the zebrafish. *Development* **129**, 2929-2946.

Olivera-Martinez, I., Harada, H., Halley, P. A. and Storey, K. G. (2012). Loss of FGF-dependent mesoderm identity and rise of endogenous retinoid signalling determine cessation of body axis elongation. *PLoS Biol.* **10**, e1001415. doi:10.1371/journal.pbio.1001415

Olivera-Martinez, I., Schurch, N., Li, R. A., Song, J., Halley, P. A., Das, R. M., Burt, D. W., Barton, G. J. and Storey, K. G. (2014). Major transcriptome re-organisation and abrupt changes in signalling, cell cycle and chromatin regulation at neural differentiation in vivo. *Development* **141**, 3266-3276. doi:10.1242/dev.112623

Palmeirim, I., Henrique, D., Ish-Horowicz, D. and Pourquié, O. (1997). Avian hairy gene expression identifies a molecular clock linked to vertebrate segmentation and somitogenesis. *Cell* **91**, 639-648. doi:10.1016/S0092-8674(00)80451-1

Pourquié, O. (2011). Vertebrate segmentation: from cyclic gene networks to scoliosis. *Cell* **145**, 650-663. doi:10.1016/j.cell.2011.05.011

Rallis, C., Pinchin, S. M. and Ish-Horowicz, D. (2010). Cell-autonomous integrin control of Wnt and Notch signalling during somitogenesis. *Development* **137**, 3591-3601. doi:10.1242/dev.050070

Rhee, J., Takahashi, Y., Saga, Y., Wilson-Rawls, J. and Rawls, A. (2003). The protocadherin papc is involved in the organization of the epithelium along the segmental border during mouse somitogenesis. *Dev. Biol.* **254**, 248-261. doi:10.1016/S0012-1606(02)00085-4

Ribes, V., Le Roux, I., Rhinn, M., Schuhbaur, B. and Dolle, P. (2009). Early mouse caudal development relies on crosstalk between retinoic acid, Shh and Fgf signalling pathways. *Development* **136**, 665-676. doi:10.1242/dev.016204

Robu, M. E., Larson, J. D., Nasevicius, A., Beiraghi, S., Brenner, C., Farber, S. A. and Ekker, S. C. (2007). p53 activation by knockdown technologies. *PLoS Genet.* **3**, e78. doi:10.1371/journal.pgen.0030078

Sawada, A., Fritz, A., Jiang, Y. J., Yamamoto, A., Yamasu, K., Kuroiwa, A., Saga, Y. and Takeda, H. (2000). Zebrafish Mesp family genes, mesp-a and mesp-b are segmentally expressed in the presomitic mesoderm, and Mesp-b confers the anterior identity to the developing somites. *Development* **127**, 1691-1702. doi:10.1242/dev.133173

Schroter, C. and Oates, A. C. (2010). Segment number and axial identity in a segmentation clock period mutant. *Curr. Biol.* **20**, 1254-1258. doi:10.1016/j.cub.2010.05.071

Schulte-Merker, S., van Eeden, F. J., Halpern, M. E., Kimmel, C. B. and Nusslein-Volhard, C. (1994). *no tail (ntl)* is the zebrafish homologue of the mouse *T (Brachyury)* gene. *Development* **120**, 1009-1015.

Selleck, M. A. and Stern, C. D. (1991). Fate mapping and cell lineage analysis of Hensen's node in the chick embryo. *Development* **112**, 615-626.

Stauber, M., Sachidanandan, C., Morgenstern, C. and Ish-Horowicz, D. (2009). Differential axial requirements for lunatic fringe and Hes7 transcription during mouse somitogenesis. *PLoS ONE* **4**, e7996. doi:10.1371/journal.pone.0007996

Takada, S., Stark, K. L., Shea, M. J., Vassileva, G., McMahon, J. A. and McMahon, A. P. (1994). Wnt-3a regulates somite and tailbud formation in the mouse embryo. *Genes Dev.* **8**, 174-189. doi:10.1101/gad.8.2.174

Takke, C. and Campos-Ortega, J. A. (1999). her1, a zebrafish pair-rule like gene, acts downstream of notch signalling to control somite development. *Development* **126**, 3005-3014.

Tam, P. P. and Tan, S. S. (1992). The somitogenetic potential of cells in the primitive streak and the tail bud of the organogenesis-stage mouse embryo. *Development* **115**, 703-715.

Team, R. R. D. C. (2009). R: A language and environment for statistical computing. R Foundation for Statistical Computing, Vienna, Austria. ISBN 3-900051-07-0, URL http://www.R-project.org.

Tzouanacou, E., Wegener, A., Wymeersch, F. J., Wilson, V. and Nicolas, J. F. (2009). Redefining the progression of lineage segregations during mammalian embryogenesis by clonal analysis. *Dev. Cell* **17**, 365-376. doi:10.1016/j.devcel.2009.08.002

Weinberg, E. S., Allende, M. L., Kelly, C. S., Abdelhamid, A., Murakami, T., Andermann, P., Doerre, O. G., Grunwald, D. J. and Riggleman, B. (1996). Developmental regulation of zebrafish MyoD in wild-type, no tail and spadetail embryos. *Development* **122**, 271-280.

Wilson, V. and Beddington, R. S. P. (1996). Cell fate and morphogenetic movement in the late mouse primitive streak. *Mech. Dev.* **55**, 79-89. doi:10.1016/0925-4773(95)00493-9

Wilson, V., Olivera-Martinez, I. and Storey, K. G. (2009). Stem cells, signals and vertebrate body axis extension. *Development* **136**, 1591-1604. doi:10.1242/dev.021246

Wymeersch, F. J., Skylaki, S., Huang, Y., Watson, J. A., Economou, C., Marek-Johnston, C., Tomlinson, S. R. and Wilson, V. (2019). Transcriptionally dynamic progenitor populations organised around a stable niche drive axial patterning. *Development* **146**, dev168161. doi:10.1242/dev.168161

Zhang, J., Bai, S., Zhang, X., Nagase, H. and Sarras, M. P.Jr (2003). The expression of gelatinase A (MMP-2) is required for normal development of zebrafish embryos. *Dev. Genes Evol.* **213**, 456-463. doi:10.1007/s00427-003-0346-4